A Novel Approach for the Investigation of Low Energy Ice Impacts

Alessia Prato[a,b,*], Marco L. Longana[b]

[a] *Politecnico di Milano, Dipartimento di Scienze e Tecnologie Aerospaziali*
[b] *University of Bristol, Bristol Composites Institute (ACCIS)*

Abstract

Soft body impacts are one of the main sources of damage for aircraft during flight due to the high relative velocities. However, a hailstone can also hit a structure at low velocity (e.g. during parking, taxi and terminal flight phases) causing barely visible damages. In this research work, a new approach is proposed for the investigation of low energy ice impacts. A drop tower apparatus was modified to accommodate specifically developed ice impactors. High-speed Digital Image Correlation was employed to measure the targets out-of-plane deformations and in-plane strain fields. Different ice impactors geometries, target materials and energy levels were considered. From results, it has been demonstrated that this methodology is able to capture the effect of ice impacting at low speed on targets.

Keywords: Low energy impact, Ice impact, Digital Image Correlation, Drop weight test
2017 MSC: 00-01, 99-00

1. Introduction

In the aeronautical field, a hailstone that hits a structure at high speed may be classified as a soft body [1]. Soft bodies are generally solids whose strength is very low compared to the target. During impacts, they lose their integrity and flow upon the target, spreading their energy on the surface. Anghileri et al. [2] discussed a numerical-experimental correlation in which hailstone impacts were studied numerically using an explicit Finite Element (FE) code (Ls-Dyna) and modelled throughout both finite elements and mesh-less approaches. A strain-rate dependent numerical model for ice, based on experimental observations, was developed by Carney at al. [3]. Experimental-numerical correlations have been also performed by Fasanella et al. [4], starting form experimental compressive tests on cylindrical ice samples. A similar approach was used by Combescure

*Corresponding author
Email address: alessia.prato@polimi.it (Alessia Prato)

et al. in [5] and a numerical model, based on dynamic experimental tests, was proposed in [6]. Numerical-experimental studies have also been conducted by Kim et al. in [7] where the authors demonstrated that a wide range of damages can be produced by hailstones impacting a structure: from barely visible (e.g. delaminations, fibre failures and through-thickness cracks) to visible impact damages (e.g. extensive through the thickness cracks and clean holes). The barely visible effect is of particular interest in composite materials, as inner delaminations can affect the functioning of a structure.

Although high energy impacts typically produce greater structural damages, low energy impacts are also of particular interest as they are not uncommon during the typical structure's life cycle. To provide an example, hailstones can strike aircraft at low speed during manoeuvring at the ground (taxing and/or parking), landing and approaching phases [8]. Moreover, it is possible to notice that during the first instants of the impact the ice behaves like a solid, cracking in compression and fragmenting [9]. During this phase, a brittle, or ductile material mechanical behaviour is shown, depending on factors such as the temperature, the strain rate, pre-stress, grain size and dispersed particles, in accordance with Shulson and Duval [10] Then, due to the high speed, it starts flowing like a fluid onto a structure, spreading its energy over an increasing portion of the target surface [9]. Recently Prato in [11] proposed a numerical methodology to investigate the solid/fluid nature of ice, based on a combined FE and Smoothed Particle Hydrodynamics (SPH).

2. Materials and Methods

The experimental approach here proposed, based on the ASTM standardised drop-weight test methodology, used to measure the impact damage resistance of Composite Fibres Reinforce Plastics (CFRP)s [12], that has been adapted to allow the use of an ice impactor. In addition to the conventional measurement prescribed by standards [12], [13] and [14], high-speed Stero DIC has been used to evaluate the target out-of-plane displacement and strain field during impact.

A schematic representation of the experimental set-up, similar to the one proposed by Hazzard et al. in [15], is shown in Figure 1. The geometry of the low test area, i.e. the target support frame, is as prescribed by the ASTM 7136 Standard [12]. Its structure is sufficiently rigid and it does not affect the deformation of the thin plates and the accuracy of DIC analysis for the maximum displacement of the plate during the tests.

Figure 1: Experimental test set-up.

2.1. Drop tower

Low energy impact tests have been performed using an Instron CEAST 9250 Drop Tower Impact System. In accordance with ASTM D7136/D7136-15 [12], a 150 mm long and 100 mm wide thin plate was clamped to the test area

and was hit by a steel impactor with a 20 mm hemispherical tip. The impact force was measured using a 15 kN piezoelectric load cell. A light-gate sensor was mounted on the drop tower to estimate the drop-weight velocity as the flag passed through it. Data were collected at a sampling frequency of 500 kHz. Pneumatic breakers were used to arrest the impactor at the desired displacement and to avoid damages to the impacting system.

As described in the ASTM standard [12], the height H necessary to achieve a certain potential energy level E is:

$$H = \frac{E}{m_d g} \tag{1}$$

where m_d is the drop weight mass and g the gravitational constant. The impact velocity v_i and the impact energy E_i can be computed from the acquired time data and flag geometry, using:

$$v_i = \frac{W_{12}}{t_2 - t_1} + g\left(t_i - \frac{(t_1 + t_2)}{2}\right) \tag{2}$$

$$E_i = \frac{m v_i^2}{2} \tag{3}$$

where the subscript i indicates a generic instant of time, W_{12} represents the length of the flag. The values t_1 and t_2 are the instants of time at which the flag passes the detecting system. Using the information of the measured impact force $F(t)$, the impactor displacement $\delta(t)$ has been obtained:

$$\delta(t) = \delta_i + v_i t + \frac{gt^2}{2} - \int_0^t \left(\int_0^t \frac{F(t)}{m} dt\right) dt \tag{4}$$

From that, the energy E_a absorbed by the target at time t can be computed as the integral of the force as a function of the displacement Equation 5 or using ASTM Standard [12], see Equation 6.

$$E_a = \int_0^\delta F(\delta) d\delta \tag{5}$$

$$E_a(t) = \frac{m(v_i^2 - v(t)^2)}{2} + mg\delta(t) \tag{6}$$

In this experimental program, the impact energy was controlled by modifying both the height and/or the mass of the drop weight.

2.2. Target structures and materials

The target structures consisted of thin plates made from different materials, see Table 1.

Table 1: Target structures' geometry and materials.

Aluminium Al6082-T6 was used in the preliminary phase to assess the procedure and verify the proper functioning of both the drop tower and the DIC. The Aluminium and the CFRPs panels were adopted as target structures during the ice impact campaign and their results were compared with impacts performed on a rigid target, made in steel.

A speckle pattern was applied to one side of each plate in order to capture the out-of-plane deformation and the strain during the tests using the DIC. More details are discussed in Section 2.4.

2.3. Ice impactors

A point of interest in this study is the creation of an ice impactor to replace the steel one prescribed by the standard [12]. To accomplish this, the following must be considered:

- It is not possible to directly connect the ice with the load cell due to the fact that the water can damage it. For this reason, a connecting structure between the ice and the load cell is required
- The connecting structure cannot be made with metallic materials, as it might affect the water freezing process
- The shape of the top section of the connector should deflect ice fragments after impact in order to prevent them from contacting with the load cell
- The shape of the bottom section should allow for a uniform growth of ice crystals during freezing and limit the number of generated defects and dislocation planes.

These considerations led to the design of a connector with the shape shown in Figure 2, which has been 3D printed with Poly-Lactic Acid (PLA). The effect of the stiffness of the connecting structure is discussed in Section 3.2. The bottom section of the connector, that is immersed into water and around which the ice forms, consist of a rounded end optimised to reduce the number of ice defects. The top section shape is conical in order to deviate ice fragments and water after the impact. Finally, the PLA was threaded to guarantee a proper connection with the drop tower.

Figure 2: Connecting structure: CAD drawing and ice impactor.

To produce the ice impactors, an ad hoc mould was designed and casted with a liquid silicon rubber (see Figure 3). This provided a smooth surface and promoted the formation of an homogeneous ice volume with a low number of inner defects.

Three ice impactor geometries were considered, inspired to the steel impactor shape. The diameter is kept constant at 20 mm, consistent with the steel impactor, whilst different lengths of the cylindrical section have been used:

- *Short body ice impactor*: the geometry is exactly the same of the steel impactor with a length of the cylindrical part equal to 10 mm
- *Medium body ice impactor*: cylindrical length of 20 mm
- *Long body ice impactor*: cylindrical length of 40 mm

Figure 3: Ice mould CAD drawing.

The effect of the impactor length on the performed tests is discussed in Section 3.2. Impactors were produced freezing distilled water at a temperature, close to 0°C, and then stored at about -20°C till their use in the experimental tests. The density of the ice was verified and it is in accordance with [10]. However, considering the difficulties in obtaining exactly the same inner structure in all the ice impactors (i.e. small inner defects and dislocation planes), only a few repetition of tests were conducted. To evaluate the ice fracture dynamics during the tests, a Photron SA-1 high-speed camera, see Figure 1, was used with a frame rate of 10 kHz.

2.4. Digital Image Correlation

Two Photron SA-Z high-speed cameras were used to perform Stereo DIC to measure the full strain field and the out-of-plane displacement of the target surface [16], [17]. Table 2 summarises the Stereo DIC set-up and the processing parameters.

Table 2: Stereo DIC main characteristics.

However, because of the spatial arrangement of the equipment, it was not possible to directly acquire images of the thin plate surface. Therefore, a mirror was placed under the test area with an angle of 45 °allowing to capture the reflected image, as shown in Figure 1 and proposed by Hazzard et al. in [15]. In this way, the displacement field ($Disp_x$, $Disp_y$, $Disp_z$) and strain field (ε_x, ε_y, ε_{xy}) of the sample surface was acquired thanks to a superficial stochastic gray-scale speckle pattern.

3. Experimental work

3.1. Steel impactor on a deformable plates

Before starting the study with ice impactors, a preliminary investigation was carried out in accordance with the prescriptions of the standards [12] using the drop tower steel impactor, see Figure 4. The aim was to investigate the response of the drop tower force-displacement curves due to changes in boundary conditions, impact energy level and target material.

Referring to the material response, for an impact energy level of 10 J, Figure 5 shows the drop tower curve results for the impact force and DIC out-of-plane

Figure 4: Steel impactor test on aluminium plate (Al 6082-T6).

displacement for the aluminium alloy and the CFRP thin plate, when subjected to a steel impact. As the impactor reaches the surface of the plate, the force curve increases and reaches a maximum value at the point of the maximum plate deflection. Table 3 presents the maximum out-of-plane deflections, measured by the drop tower as impactor displacement, and the DIC values as the material displacement.

Table 3: Investigation on materials' response (energy level of 10 J): comparison of the maximum out-of-plane displacements.

The difference between the DT and DIC out-of-plane displacement can be ascribed to the accuracy of both the measurement systems and intrinsic errors. In particular the displacement obtained by the drop tower was indirectly measured from Equation 4. As in [15], the DIC accuracy was also affected by the indirect capture of the target plate out of plane displacement due to the use of a mirror, which reflected and projected the superficial speckle pattern.

Figure 5: Investigation on materials' response (energy level of 10 J): impact force and DIC maximum out-of-plane displacement. The DIC images are centred in the impacted area.

The effect of the impact energy level was also considered in this preliminary study. Referring to Figure 6, on 1.5 mm thick aluminium plates, an increment of impact energy produced an increase in force and maximum out-of-plane displacement.

Figure 6: Effect of impact energy level (aluminium plates 1.5 mm thick). Impact forces, DIC maximum out-of-plane displacements and strain maps. The DIC images are centred in the impacted area.

Table 4 shows a comparison between the maximum out-of-plane deflection of the drop tower and the DIC, as the energy level changed.

Table 4: Effect of impact energy level (aluminium plates 1.5 mm thick): comparison of the maximum out-of-plane displacements.

3.2. Preliminary investigation on ice impactors' geometry

Three ice impactor geometries have been considered, as discussed in Section 2.3.

From the drop tower recording, it was observed that, when the short body ice impactor was used, the pneumatic breaks were not able to engage before the connecting structure came into contact with the target plate. This produced a

permanent deformation of the aluminium plate and damaged the PLA component, resulting in an increment of the energy and force recorded by the drop tower acquisition system, as shown in Figure 7.

Figure 7: Short body ice impactor: effect of impact energy level (aluminium plates 1.5 mm thick) with impact of ice and PLA connecting structure.

On the contrary, the long ice impactor, because of its slender shape, completely lost its integrity at the first contact with the target without transferring a significant amount of energy to the plate. An example is provided in Figure 8. As the length of the cylindrical part increased, failures were found to occur earlier and, consequently, the amount of admissible data was reduced.

Figure 8: Brittle failure of the long body ice impactor: frames from high speed video recording. The time is computed from the first instant of impact.

In conclusion, the use of the medium body ice impactor was found to provide the best solution: a compromise between an impactor geometrically similar to the one proposed by the standards and sufficient ice to avoid impact of the PLA structure, without completely destroying the all ice impactor during first contact with the plate.

This initial investigation, carried out with thin aluminium alloy plate, was used to study the qualitative behaviour of ice during low energy impact. From that, the medium body ice impactor was selected and used to investigate the effect of low energy ice impact against different target materials.

Figure 9: Brittle failure of the medium body ice impactor: frames from high speed video recording. The time is computed from the first instant of impact.

Also, the ice started cracking after the first impact allowing the energy to be absorbed by both the ice and the plate deformation.

Figure 9 shows a sequence of frames taken from the video recording of the medium body ice impactor hitting the aluminium plate. The brittle nature of ice emerged and the fluid like behaviour, tipical of high speed impact [1], [9], was not observed. Also, the ice started cracking after the first impact allowing the energy to be absorbed by both the ice and the plate deformation. Therefore, the connecting structure did not have any active part in the test and a negligible part of the energy was absorbed by it.

3.3. Ice impact on a thick steel plate

A series of tests using a thick steel plate as target structure was performed to evaluate the behaviour of the impactor structure on a not deformable plate. More in details, due to the absence of plastic deformation or failure of the target, the drop tower recorded only the response of the ice and of the connecting

Table 5: Steel target: experimental results.

Figure 10: Steel target: force curve response.

structure. Results, in terms of peak of force and absorbed energy, see Equation 5, are presented in Table 5

In general, as the impact energy increased, both the total energy and the peak of force increased. Lower values in both parameters were observed when the test was performed at 75 J, see Figure 10. This was due to a premature failure of the ice due to a greater number of inner defects. Note that DIC was not conducted, as no deformation of the steel plate occurred.

3.4. Ice impact on thin aluminium plates

The use of thin aluminium plates as a target implies the introduction of the plastic deformation of the panel. Consequently, the contribution of the plate to the energy absorption properties must be taken into account. In addition, the deformation of the aluminium allows the use of the DIC to evaluate the displacement and deformation.

Figure 11: Aluminium target: impact force, DIC out-of-plane displacements and strain. The DIC images are centred in the impacted area.

Figure 11 shows the drop tower result for an impact energy of 30 J and the corresponding out-of-plane displacement and strain. The estimated value of maximum displacement was 0.40 mm, whilst the value obtained from the DIC was equal to 0.75 mm. In Table 6 the main results are shown for different impact energy levels.

Table 6: Aluminium target: experimental results.

3.5. Ice impact on thin composite plates

A similar approach was used for the analysis of a CFRP thin laminate, whose main characteristics were presented in Table 1. Figure 12 shows the drop tower force result for an impact energy of 50 J and the corresponding out-of-plane displacement and strain of the plate obtained from the DIC analysis.

Figure 12: Composite target: impact force, DIC out-of-plane displacements and strain. The DIC images are centred in the impacted area.

The estimated value of maximum displacement computed (1.37 mm) is not so far from the value obtained by the DIC (1.18 mm). Looking at Table 7, it is possible to see that the discrepancy in data results, as previously discussed, can be attributed to the non homogeneity of the ice structure.

Table 7: Composite target: experimental results.

3.6. Results overview

The approach proposed here for the investigation of low energy ice impact allowed to fully capture the solid nature of ice throughout its brittle failure. This is hardly achievable with typical high-speed impact tests, in which the ice is threaded like a fluid [1]. From a qualitative point of view, the brittle rupture of ice clearly appears in all the tests, as shown in Figure 8 and Figure 9. This can be attributed to:

- *Velocity*: the tests were performed at a velocity lower than 5 m/s, inhibiting the ice from showing any hydrodynamic behaviour and making its solid response dominant [1] [9]
- *Temperature*: the ice impactors were stored, before the tests, at approximately -21°C, i.e. the ductile-to-brittle transition temperature [10]
- *Defects*: it was very difficult to produce ice impactors free from inner defects, these represented a preferential failure initiation point, allowing the brittle failure to begin at the first contact with the target plate.

It should be remarked that, despite the fact that all the ice impactors underwent the same freezing process and storing conditions, it was almost impossible to achieve a completely uniform ice structure. Differences in both macroscopic and microscopic defects were observed, making the test repeatability difficult.

The use of an experimental set-up derived from the ASTM 7136 [12] standard allows obtaining for a brittle impactor, such as the ice, the same set of information obtainable for the steel impactor as prescribed by the standard. This allows, if not a direct comparison of the results obtained using impactors of different nature, a step forward towards a more comprehensive investigation of the effects of soft bodies, and in particular ice, impacts on engineering structures.

The use of high-speed stereo DIC enabled, during the whole impact event, the tracking of the out of plane deflection and the evaluation of the full-strain field. As from results, a drawback was related to the difference that occurred between the drop tower and the DIC out-of-plane displacement evaluation. For ice impact tests, this was due to the fact that the drop tower provide as a result the displacement of the impactor that did not follow the real displacement of the target surface, as instead was done by the DIC. However, this technique provided further information on the effect of ice impacts on different target structures (i.e. aluminium and composite thin plates).

Figure 13: Comparison of peak of force from the ice impact tests performed against different target materials.

Specifically, an interesting aspect was the effective absorption capability of the materials when undergoing ice impacts. A direct comparison between the tests performed on steel, aluminium and composite target plates is presented in Figure 13. Despite the significative data dispersion, the line plots provide a qualitative trend of the force peak values as the energy level increases. In general, for stiffer targets, a higher value of the impact force was reached. From results, the composite material seemed to absorb a greater amount of energy compared to the aluminium target, even if it must be kept in mind that the ice, because of its brittle behaviour, absorbs part of the impact energy.

4. Conclusions

In this research activity, a novel approach was used to simulate low energy ice impacts. This allowed the evaluation of the mechanical behaviour of the ice impactor and a comparison between the response of different target structures.

For the experimental set-up, a drop tower was used to collect force and displacement data under controlled conditions. The high-speed stereo DIC allowed to evaluate the deformation of the thin target plates and a third high speed camera was used to visualise ice fracture during impact events. This experimental set-up made possible to observe the brittle failure of ice impactor and its solid nature during low energy impacts.

The ice impactor shape, inspired by the one prescribed by standard ASTM [12], was optimised to avoid premature failure. However, accuracy of the results was affected by the fact that it was not possible to produce perfectly consistent ice impactors without inner defects. An optimisation of the freezing cycle is therefore required and will be object of further studies.

The development of this experimental program allowed the evaluation of the energy absorbed by the target during an ice impact. For the same initial conditions, the composite material displayed improved energy absorption capability over the aluminium target.

Additional tests will be conducted to evaluate the absorption capabilities due to soft body, i.e. ice, impacts of different target materials. Moreover, soft not brittle impactor will be considered in further investigations.

Acknowledgements

The authors would like to thank Professor Anghileri, Professor of the Aerospace Science and Technology Department of Politecnico di Milano, and Professor Wisnom, Director of the Bristol Composites Institute (ACCIS).

References

[1] J. S. Wilbeck, Impact behaviour of low strength projectiles, report afml-tr- 77-134, Tech. rep., Air Force Material Laboratory, Air Force Wright Aeronautical Laboratories, Air Force System Command, Wright Patterson Air Force Base (1977).

[2] M. Anghileri, L. Castelletti, F. Invernizzi, M. Mascheroni, A survay of numerical models for hail impact analysis using explicit finite element codes, International Journal of Impact Engineering 31(8) (2005) 929–944. doi:10.1016/j.ijimpeng.2004.06.009.

[3] K. Carney, D. Benson, P. Du Bois, R. Lee, A phenomenological high strain rate model with failure for ice, International Journal of Solid and Structures 43 (2006) 7820–7839. doi:10.1016/j.ijsolstr.2006.04.005.

[4] E. Fasanella, R. Boitnott, S. Kellas, Test and analysis correlation of high speed impacts of ice cylinders, 9th International Ls-Dyna Users Conference, Detroit, USA, 2006.

[5] A. Combescure, Y. Chuzel-Mamot, J. Fabis, Experimental study of high velocity impact and fracture of ice, International Journal of Solids and Structures 48 (2011) 2779–2790. doi:10.1016/j.ijsolstr.2011.05.028.

[6] Y. Chuzel, M. Combescure, A. snd Nucci, R. Ortiz, Y. Perrin, Development of hail material model for high speed impacts on aircraft engine, 11th International Ls-Dyna User Conference, Detroit, USA, 2010.

[7] H. Kim, D. Welch, K. Kedward, Experimental investigation of high velocity ice impacts on woven carbon/epoxy composite panels, Composite Part A 34 (2003) 25–41. doi:10.1016/S1359-835X(02)00258-0.

[8] Faa, Faa aviation safety information analysis and sharing (Asias), weather-related aviation accident study (2003-2007), Tech. rep., Federal Aviation Administration, http://www.asias.faa.gov/ (2010).

[9] J. Tippmann, H. Kim, J. Rhymer, Experimentally validated strain rate dependent material model for spherical ice impact simulation, International Journal of Impact Engineering 55 (2013) 43–54. doi:10.1016/j.ijimpeng.2013.01.013.

[10] E. M. Schulson, P. Duval, Creep and Fracture of Ice, Cambridge University Press, 2009.

[11] A. Prato, M. Anghileri, A. Milanese, L. Castelletti, Fe-to-Sph approach applied to the analysis of soft body impact: Bird strike and hail impact, 29th International Aeronautical and Astronautical Council Conference (ICAS 2014), St. Petersburg, Russia, 2014.

[12] Standard test method for measuring the damage resistance of a fiber-reinforced polymer matrix composite to a drop-weight impact event, Astm D7136/D7136M-15, Tech. rep., Astm International (2015).

[13] Standard test method for high speed puncture properties of plastics using load and displacement sensors, Astm D3763-15, Tech. rep., Astm International (2015).

[14] Plastics determination of puncture impact behaviour of rigid plastics - part 2: Instrumented impact testing, ISO 6603-02, Tech. rep., International Standard (2000).

[15] M. Hazzard, S. Hallett, P. Curtis, L. Iannucci, R. Trask, Effect offibre orientation on the low velocity impact response of thin dyneema®composite laminates, International Journal of Impact Engineering 100 (2017) 35–45. doi:10.1016/j.ijimpeng.2016.10.007.

[16] B. Pan, K. Quian, H. Xie, A. Asundi, Two dimensional digital image correlation for in-plane displacement and strain measurement: a review, Measurement Science and Technology 20(6) (2009) 1–17. doi:10.1088/0957-0233/20/6/062001.

[17] M. Longana, J. Dulieu-Barton, F. Pierron, Identification of constitutive properties of composite materials under high strain rate loading using optical strain measurement techniques, 15th European Conference on Composite Materials, Venice, Italy, 2012.

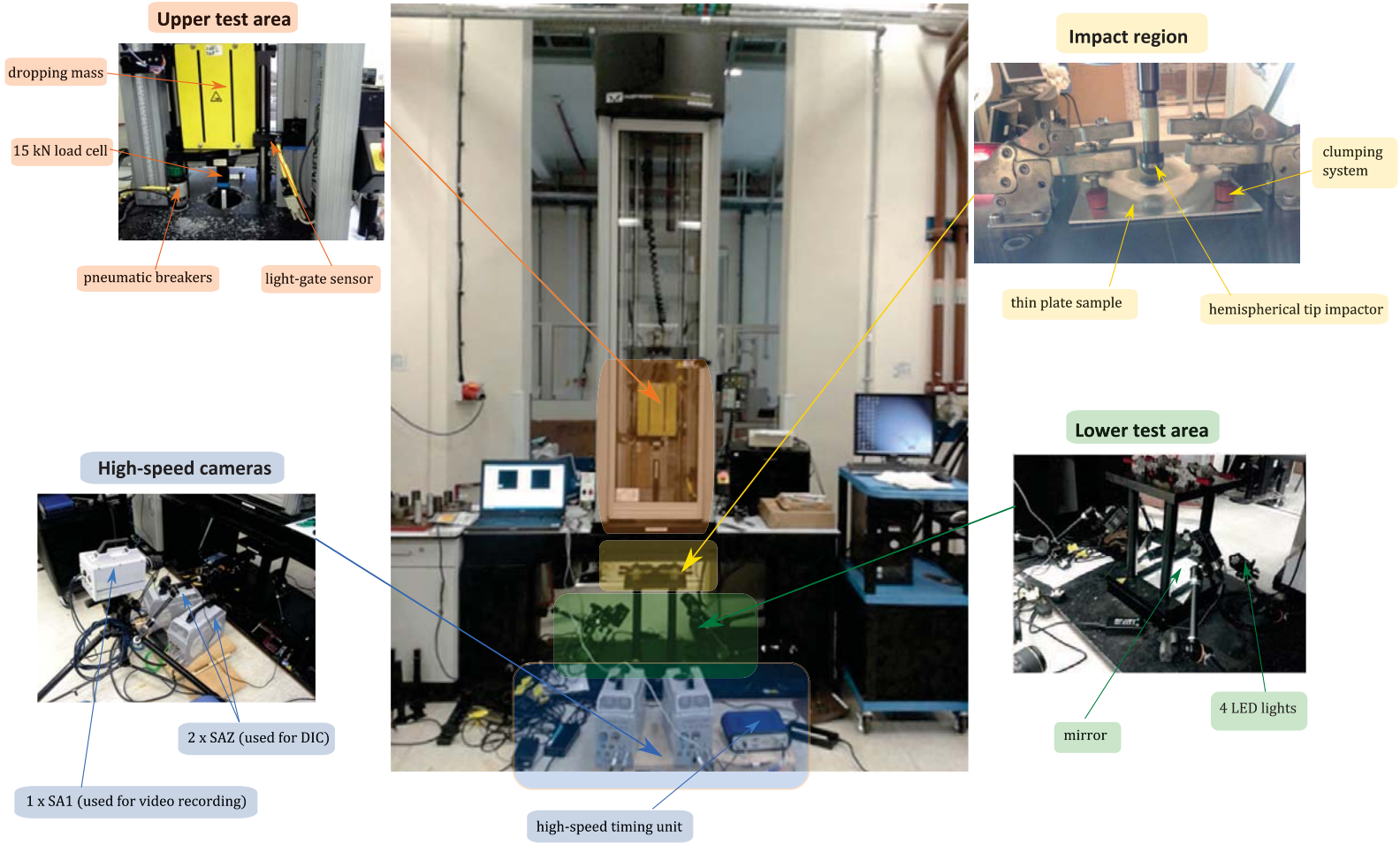
Upper test area
dropping mass
15 kN load cell
pneumatic breakers
light-gate sensor
Impact region
clumping system
thin plate sample
hemispherical tip impactor
Lower test area
4 LED lights
mirror
High-speed cameras
2 x SAZ (used for DIC)
1 x SA1 (used for video recording)
high-speed timing unit

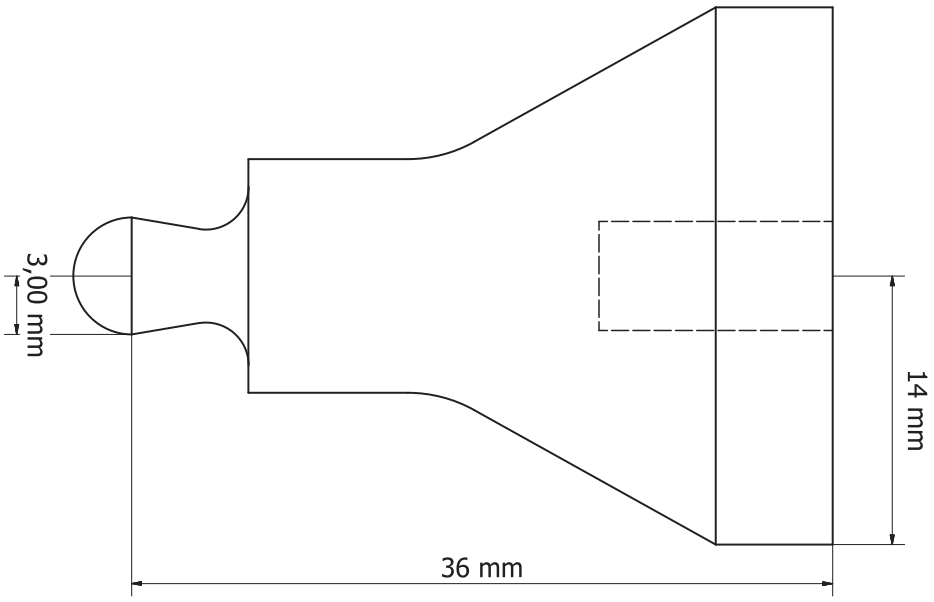
3,00 mm
14 mm
36 mm

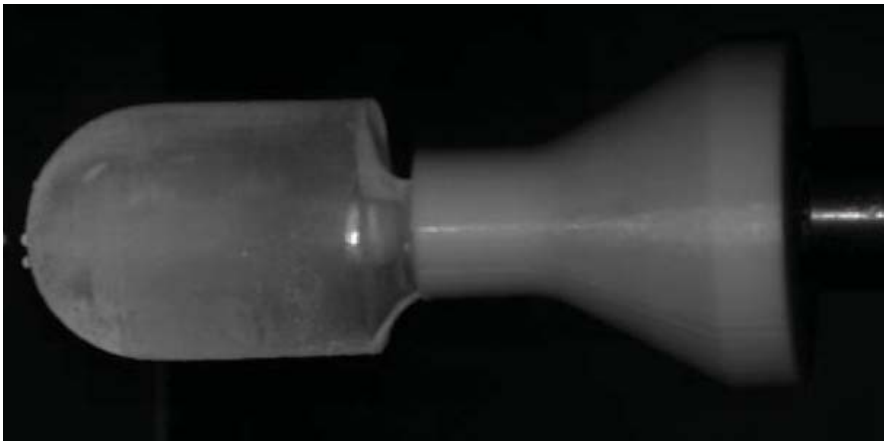

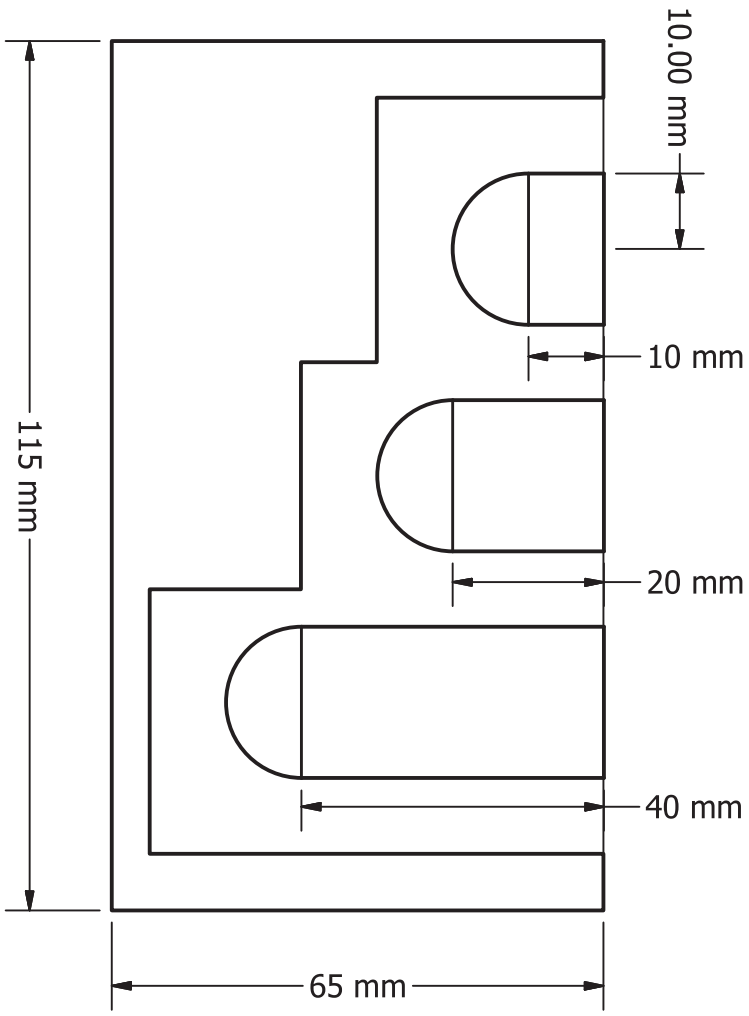
10.00 mm
10 mm
20 mm
40 mm
115 mm
65 mm

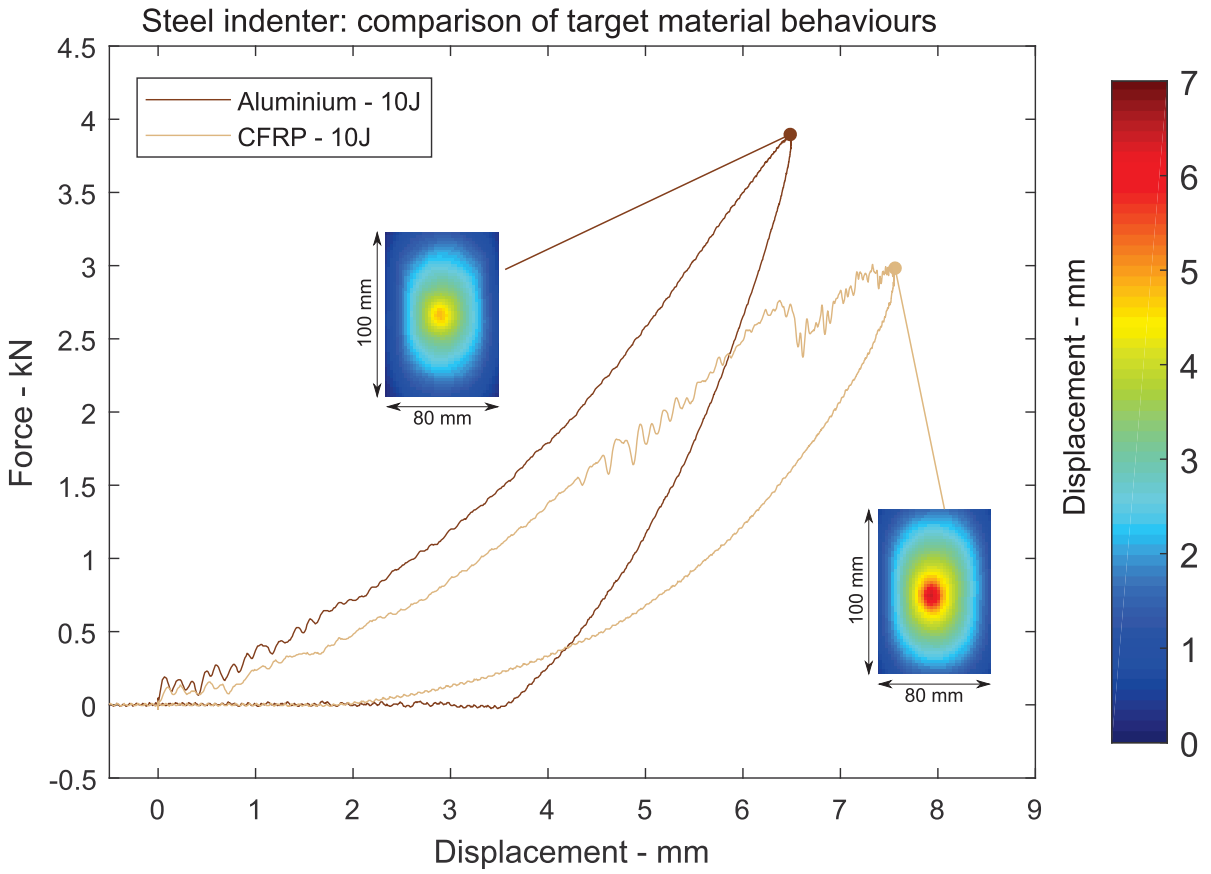
Steel indenter: comparison of target material behaviours
Aluminium - 10J
CFRP - 10J
Force - kN
Displacement - mm
Displacement - mm
100 mm
80 mm
100 mm
80 mm
4.5
4
3.5
3
2.5
2
1.5
1
0.5
0
-0.5
0
1
2
3
4
5
6
7
8
9
7
6
5
4
3
2
1
0

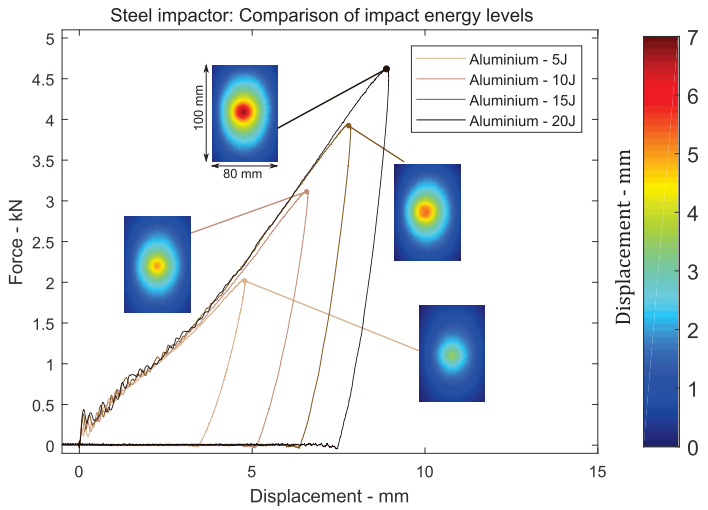
Steel impactor: Comparison of impact energy levels
Aluminium - 5J
Aluminium - 10J
Aluminium - 15J
Aluminium - 20J
100 mm
80 mm
Force - kN
Displacement - mm
Displacement - mm
0
1
2
3
4
5
6
7
0
0.5
1
1.5
2
2.5
3
3.5
4
4.5
5
0
5
10
15

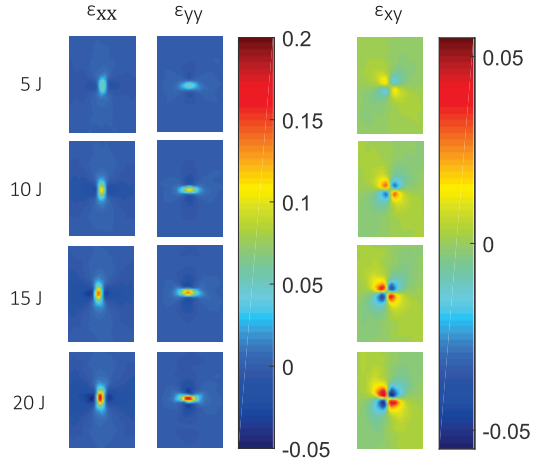
εxx
εyy
εxy
5 J
10 J
15 J
20 J
0.2
0.15
0.1
0.05
0
-0.05
0.05
0
-0.05

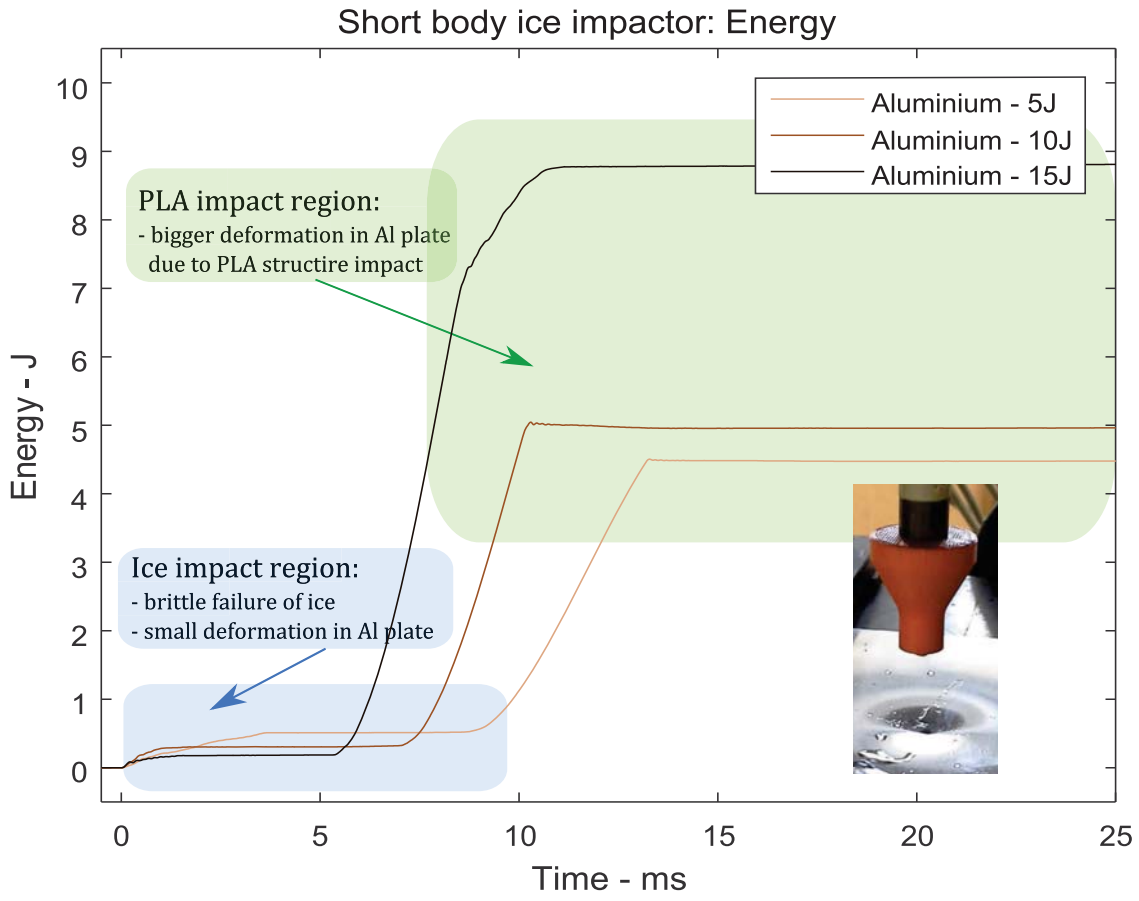
Short body ice impactor: Energy
Aluminium - 5J
Aluminium - 10J
Aluminium - 15J
PLA impact region:
- bigger deformation in Al plate
due to PLA structire impact
Ice impact region:
- brittle failure of ice
- small deformation in Al plate
Energy - J
Time - ms
0
1
2
3
4
5
6
7
8
9
10
0
5
10
15
20
25

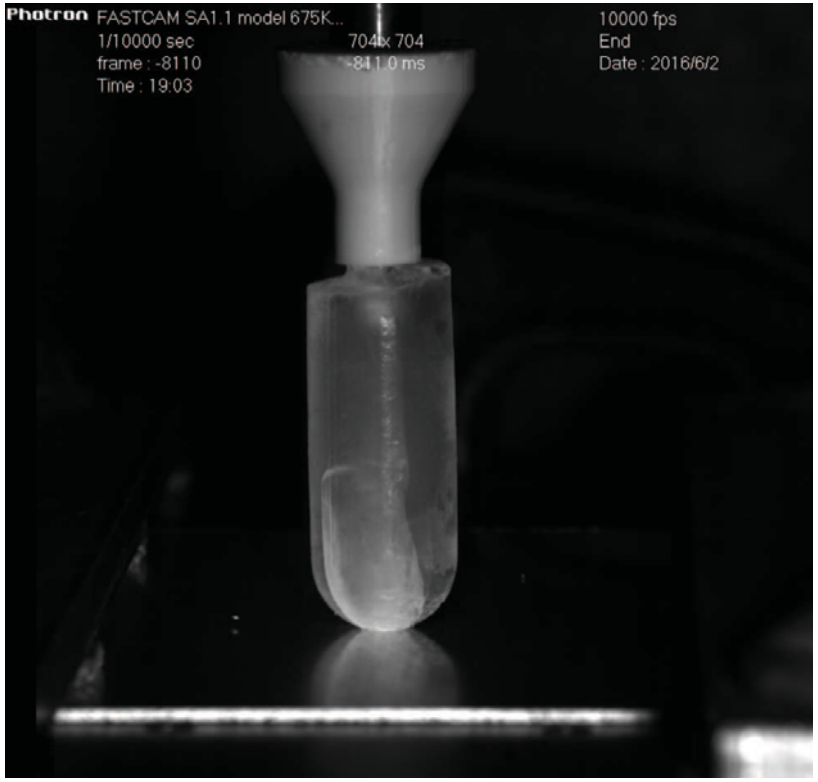
Photron FASTCAM SA1.1 model 675K...
1/10000 sec
frame : -8110
Time : 19:03
704x 704
-841.0 ms
10000 fps
End
Date : 2016/6/2

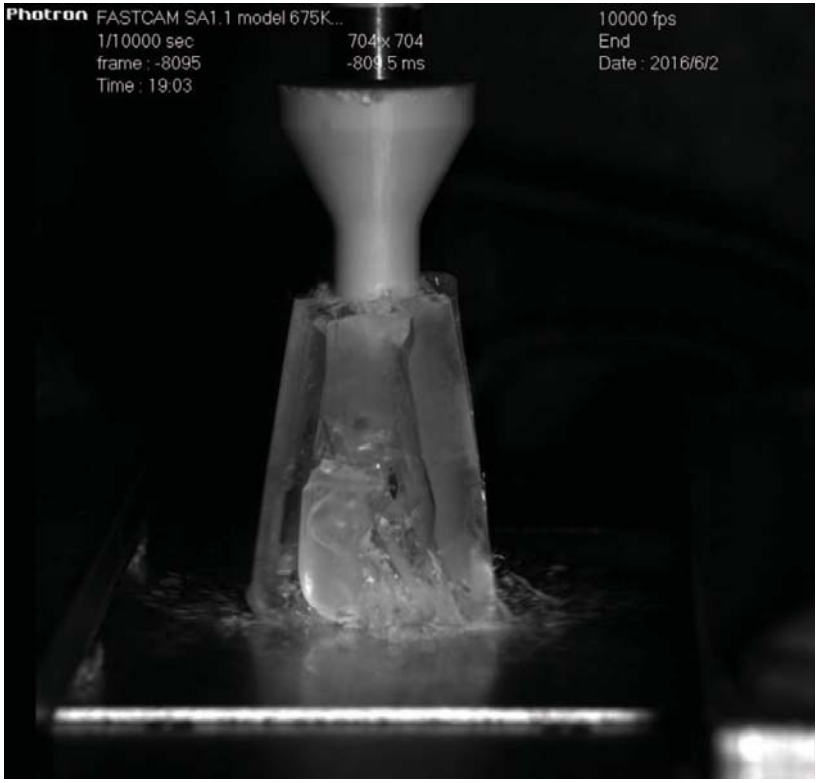
Photron FASTCAM SA1.1 model 675K...
1/10000 sec
frame : -8095
Time : 19:03
704 x 704
-809.5 ms
10000 fps
End
Date : 2016/6/2

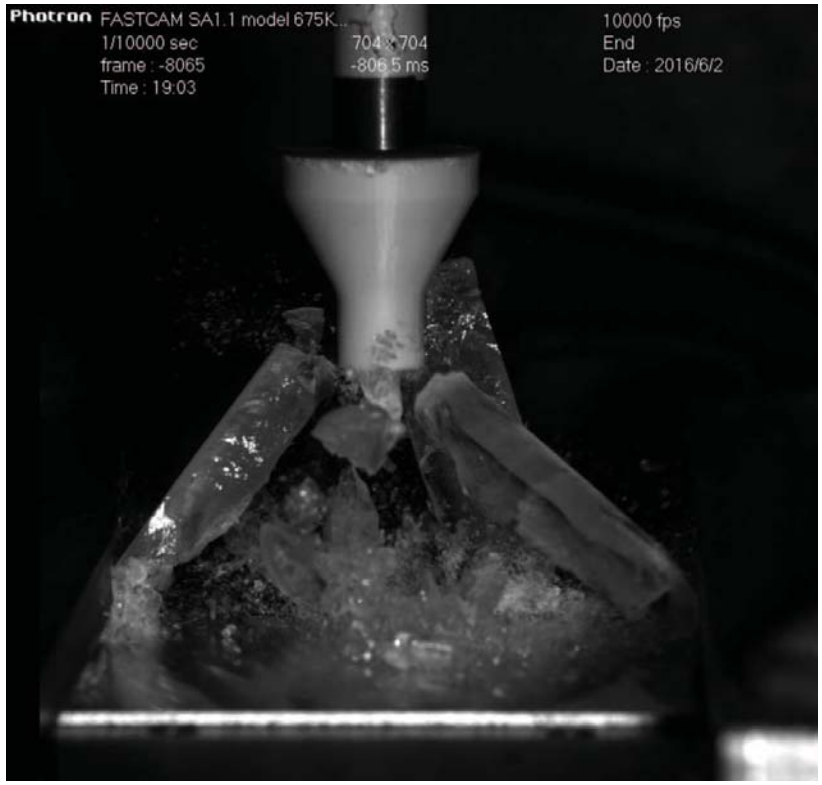
Photron FASTCAM SA1.1 model 675K...
1/10000 sec
frame : -8065
Time : 19:03
704 x 704
-806.5 ms
10000 fps
End
Date : 2016/6/2

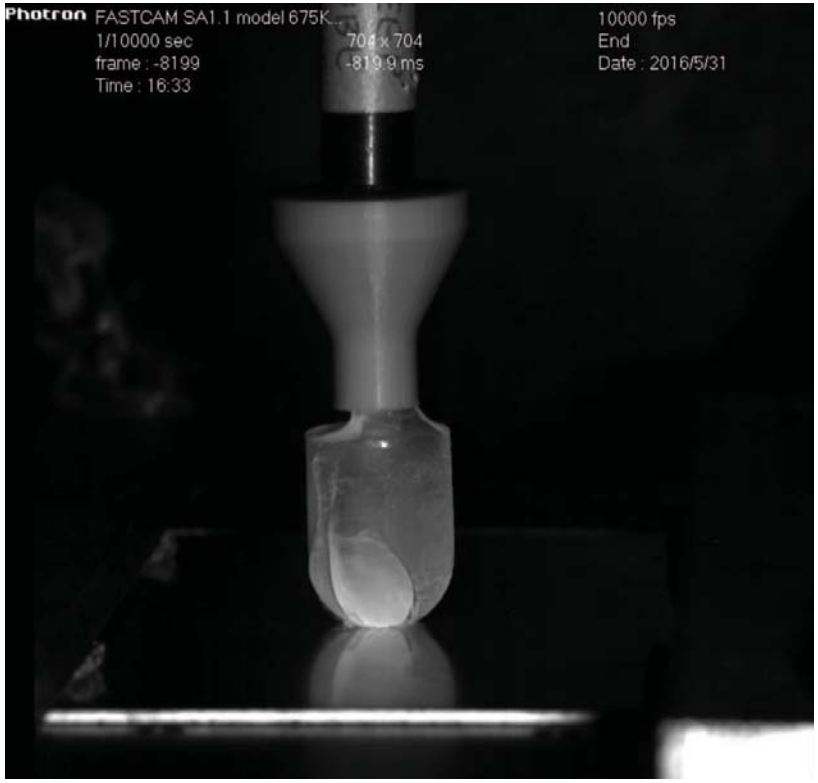
Photron FASTCAM SA1.1 model 675K...
1/10000 sec
frame : -8199
Time : 16:33
704 x 704
-819.9 ms
10000 fps
End
Date : 2016/5/31

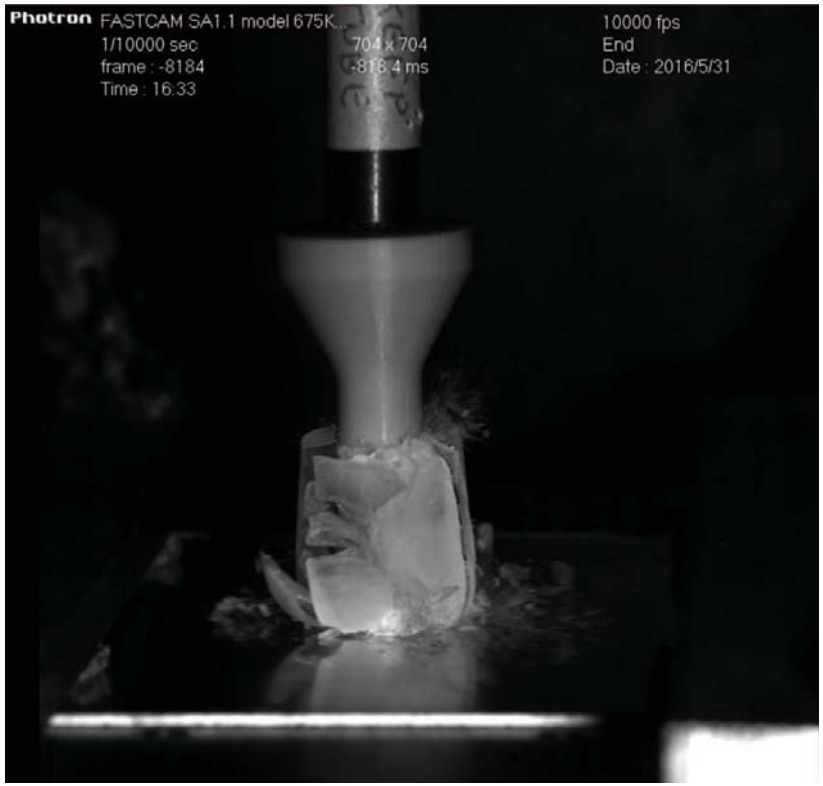
Photron FASTCAM SA1.1 model 675K...
1/10000 sec
frame : -8184
Time : 16:33
704 x 704
-818.4 ms
10000 fps
End
Date : 2016/5/31

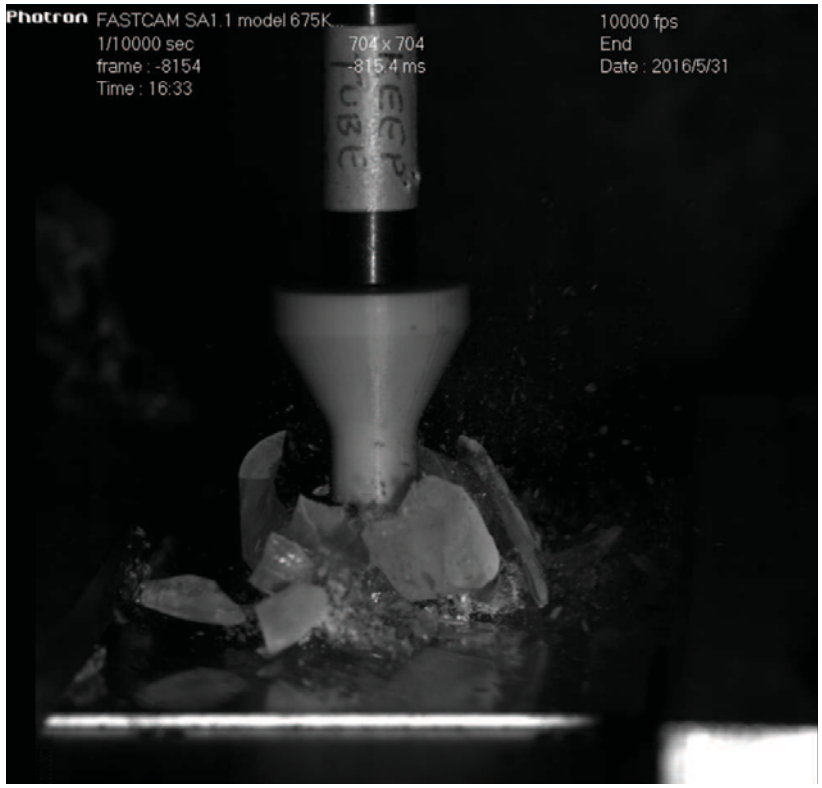
Photron FASTCAM SA1.1 model 675K
1/10000 sec
frame : -8154
Time : 16:33
704 x 704
-815.4 ms
10000 fps
End
Date : 2016/5/31

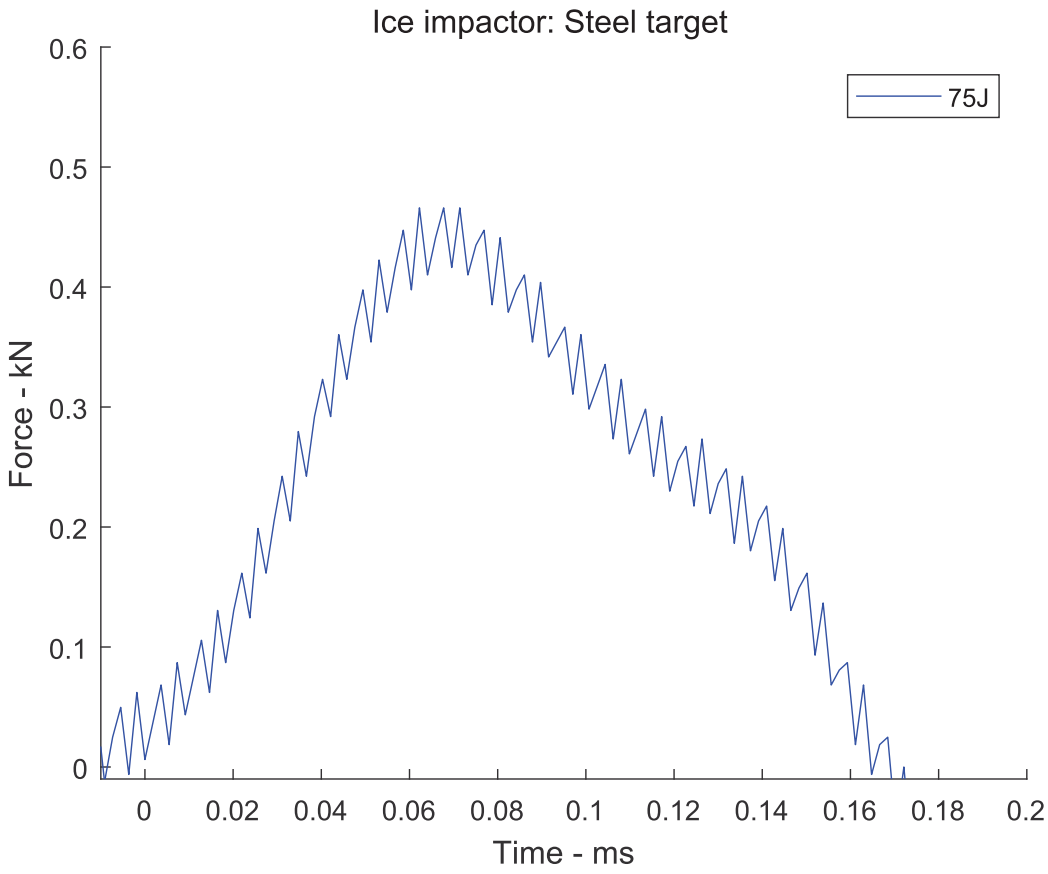
Ice impactor: Steel target
75J
Force - kN
Time - ms
0
0.1
0.2
0.3
0.4
0.5
0.6
0
0.02
0.04
0.06
0.08
0.1
0.12
0.14
0.16
0.18
0.2

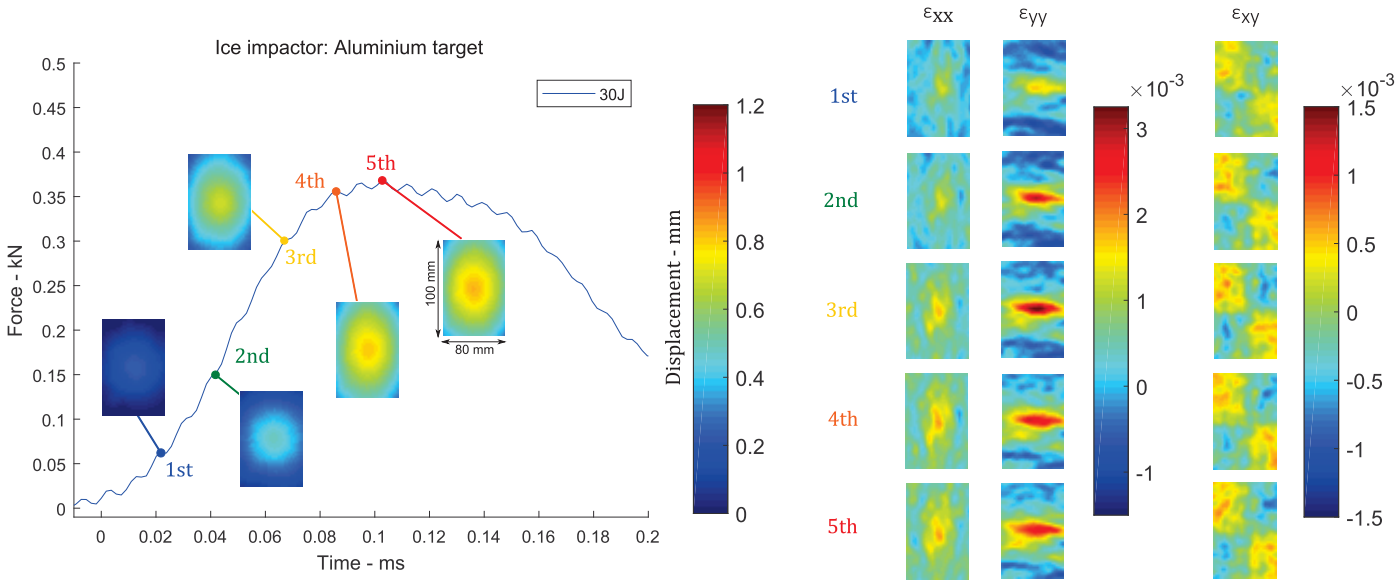
Ice impactor: Aluminium target
30J
Force - kN
Time - ms
Displacement - mm
100 mm
80 mm
1st
2nd
3rd
4th
5th
εxx
εyy
εxy
×10-3

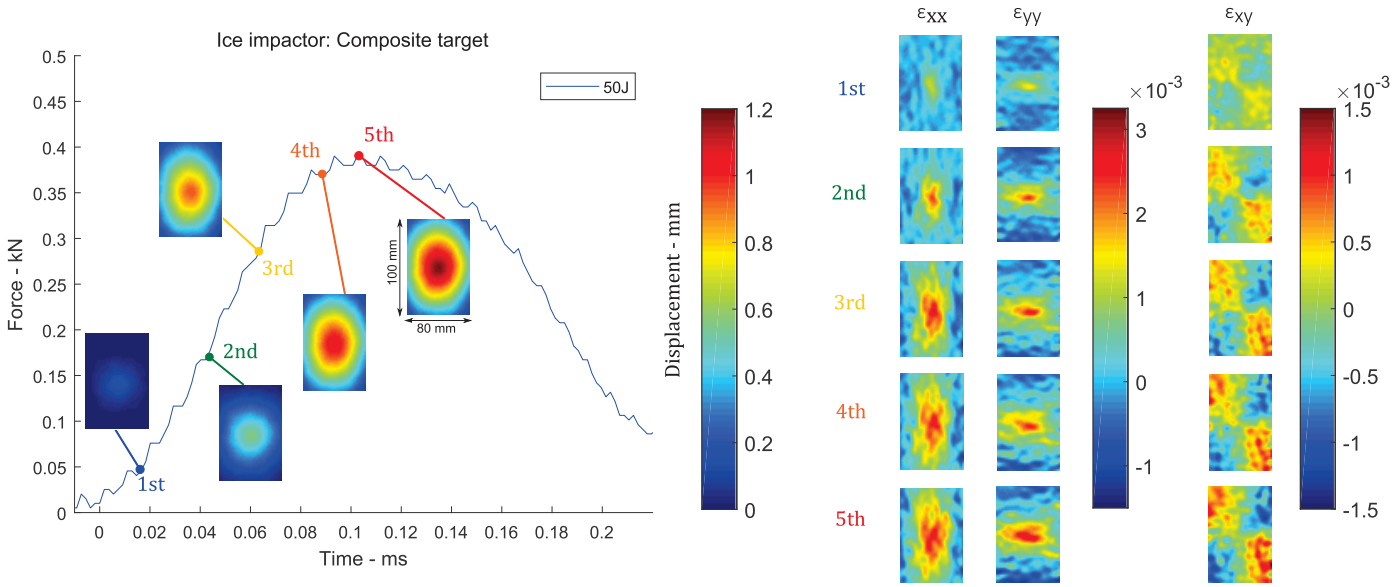
Ice impactor: Composite target
50J
Force - kN
Time - ms
1st
2nd
3rd
4th
5th
100 mm
80 mm
Displacement - mm
εxx
εyy
εxy
×10-3
×10-3

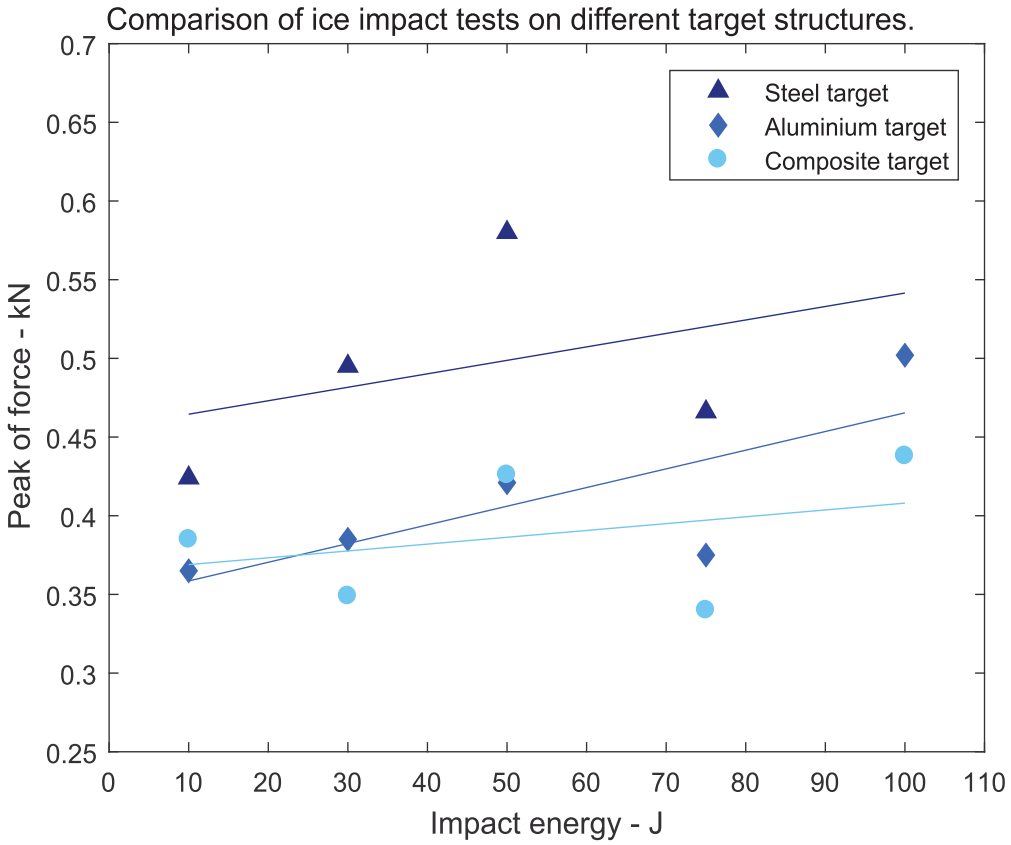
Comparison of ice impact tests on different target structures.
Steel target
Aluminium target
Composite target
Peak of force - kN
Impact energy - J
0.7
0.65
0.6
0.55
0.5
0.45
0.4
0.35
0.3
0.25
0
10
20
30
40
50
60
70
80
90
100
110

Characteristic	**Steel Fe360**	**Al 6082-T6**	**CFRP [0-90]$_8$**
Dimensions $-mm$	200x200	110x150	110x150
Thickness $-mm$	15.0	1.0, 1.5	1.5
Density $-kg/m^3$	7800	2400	1180
Elastic modulus $-MPa$	198000	72000	57000
Poisson coefficient $-$	0.28	0.33	0.30
Yield stress $-MPa$	300	239	-
Ultimate tensile stress $-MPa$	440	310	876

Table 1: Target structures' geometry and materials.

Characteristic	**Set-up**
Technique used	3D DIC
Subsetsize	31x31 $pixels$
Stepsize	10 $pixels$
Camera	Photron SA-Z
Lens	Tonika AT-X Pro Macro 100 F2.8 D
Resolution	1024x1024 $pixels$
Field of view	104x147 mm
Frame rate	32 kHz
Spatial resolution	1.62 mm
Displacement resolution	0.0019 mm
Strain resolution	68 $\mu\varepsilon$

Table 2: Stereo DIC main characteristics.

Material	**Out-of-plane displacement** mm	
	Drop tower	**DIC**
Aluminium	6.49	4.80
CFRP	7.55	6.40

Table 3: Investigation on materials' response (energy level of 10 J): comparison of the maximum out-of-plane displacements.

Energy level J	**Out-of-plane displacement** mm	
	Drop tower	**DIC**
5	4.79	3.45
10	6.61	4.98
15	7.85	5.26
20	8.94	6.74

Table 4: Effect of impact energy level (aluminium plates 1.5 mm thick): comparison of the maximum out-of-plane displacements.

Impact energy J	**Total energy** J	**Peak of Force** kN
10.00	0.10	0.42
30.00	0.18	0.50
50.00	0.21	0.58
75.00	0.13	0.47

Table 5: Steel target: experimental results.

Impact energy J	**Total energy** J	**Peak of Force** kN	**Out-of-plane displacement** mm	
			Drop tower	**DIC**
10.00	0.23	0.37	1.06	0.77
30.00	0.32	0.39	1.06	0.83
50.00	0.22	0.42	0.40	0.76
75.00	0.18	0.38	0.28	-
100.00	0.83	0.50	1.26	-

Table 6: Aluminium target: experimental results.

Impact energy J	**Total energy** J	**Peak of Force** kN	**Out-of-plane displacement** mm	
			Drop tower	**DIC**
10.00	0.36	0.39	1.15	-
30.00	0.86	0.35	1.12	1.04
50.00	0.59	0.43	1.37	1.18
75.00	0.48	0.34	1.24	-
100.00	0.39	0.44	1.35	-

Table 7: Composite target: experimental results.